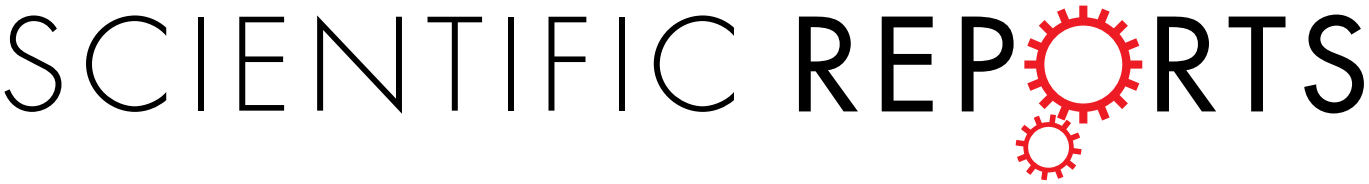

OPEN

Direct Synthesis of cubic shaped Ag_2S on Ni mesh as Binder-free Electrodes for Energy Storage Applications

Received: 25 March 2019
Accepted: 21 June 2019
Published online: 12 July 2019

Arunachalam Arulraj[1], N. Ilayaraja[2], V. Rajeshkumar[3] & M. Ramesh[2]

A facile approach of chemical bath deposition was proposed to fabricate direct synthesis of silver sulphide (Ag_2S) on nickel (Ni) mesh without involvement for binders for supercapacitor electrodes. The phase purity, structure, composition, morphology, microstructure of the as-fabricated Ag_2S electrode was validated from its corresponding comprehensive characterization tools. The electrochemical characteristics of the Ag_2S electrodes were evaluated by recording the electrochemical measurements such as cyclic voltammetry and charge/discharge profile in a three electrode configuration system. Ag_2S employed as working electrode demonstrates notable faradaic behaviour including high reversible specific capacitance value of 179 C/g at a constant charge/discharge current density of 1 A/g with high cyclic stability which is relatively good as compared with other sulphide based materials. The experimental results ensure fabricated binder-free Ag_2S electrodes exhibits better electrochemical performance and suitable for potential electrodes in electrochemical energy storage applications.

In the past few decades, considerable research efforts have been focused on alternative energy storage and conversion devices with significant efficiency with low cost such as batteries, solar cells, fuel cells, electrochemical capacitors etc[1–3]. Among these, electrochemical capacitors commonly known as supercapacitors, have been known for promising energy storage devices owing to its uniqueness such as high power density, outstanding reversibility, rapid recharge ability, extended life cycle and low cost fabrication[4,5]. These properties have drawn much attention as energy devices in addition to that of batteries. Even though, supercapacitors have smaller energy densities than batteries, it has a potential of delivering high power density owing to its rapid ion exchange process[6]. The mechanism of energy storage in supercapacitors is inherently rapid because it involves simple ions movement to and fro on the electrode surfaces. Based on the charge storage mechanism, it is broadly classified into two type viz.: (i) Pseudocapacitors (PSCs) and (ii) Electrical double layer capacitors (EDLCs). Currently, EDLCs exhibit higher power density, but it suffers from lower energy density, while PSCs possess a high specific capacitance value of 10–100 times higher than that of EDLCs[7–9].

Recently, layered type transition metal chalcogenides (TMC), metal carbides and metal nitrides are demonstrated as elevated staging supercapacitive materials[10–13]. Similarly, other transition metal chalcogenides such as NiS, CoS, CuS and ternary metal sulphides are explored as better pesudocapacitive materials[14,15]. The sulphide based materials exhibits excellent electronic, physio-chemical and good conductivity properties, which can serves as an alternative electrode for energy storage applications. Ag_2S belonging to I–VI compound semiconductor with the band gap of 1–2 eV is one of the promising material for energy storage and conversion devices. Owing to its photo-electric, bandgap and thermal properties it finds own path in different applications such as IR detectors, photoconductors etc[16–18]. In general, fabrication of metal chalcogenides thin films can be deposited on different substrates using various physicochemical techniques like Chemical Vapour Deposition, SILAR, Electrodeposition and so on. Among the other techniques, Chemical Bath Deposition (CBD) in aqueous medium is one the simplest and most economical route to prepare Ag_2S thin films. CBD, technique has more advantages like low temperature aqueous method for depositing large-area thin films of semiconductors with good uniformity and better

[1]Department of Physics, University College of Engineering – Bharathidasan Institute of Technology (BIT) campus, Anna University, Tiruchirappalli, India. [2]Functional Materials Division, CSIR- Central Electrochemical Research Institute (CECRI), Karaikudi, India. [3]Department of Chemistry, National Institute of Technology, Tiruchirappalli, India. Correspondence and requests for materials should be addressed to M.R. (email: rameshpondi108@gmail.com)

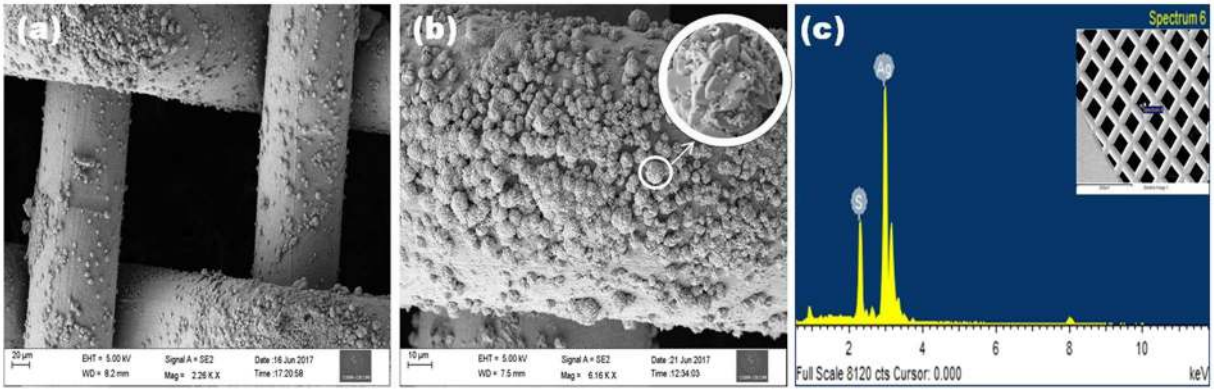

Figure 1. FESEM images of (**a**) Ag_2S deposited on Ni mesh, (**b**) magnified image and (**c**) EDAX spectrum of Ag_2S.

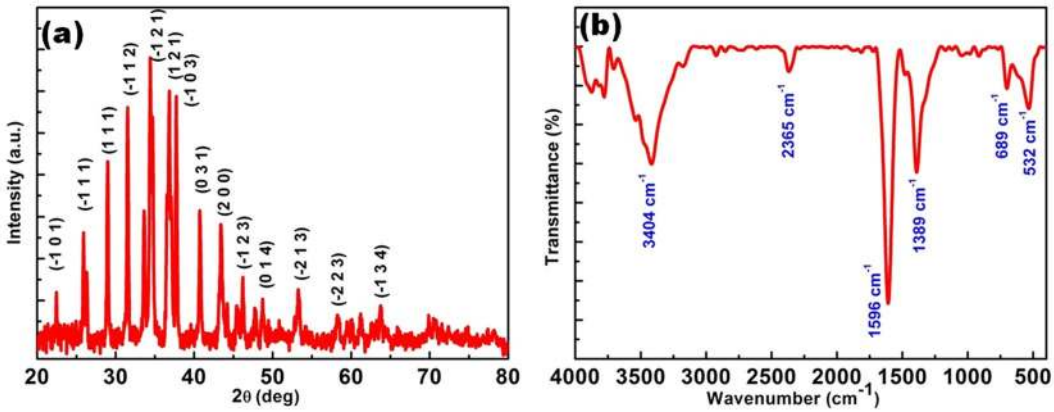

Figure 2. (**a**) XRD pattern and (**b**) FT-IR spectrum of chemical bath synthesized Ag_2S.

adhesion than the others. Besides, it does not require any vacuum system or sophisticated instrument and also the starting materials used in this present work are commonly available and much cheap. Dhumere *et al*. studied the effect of bath temperature and addition of complexing agent on deposition of Ag_2S thin films using CBD method[19]. Followed by Dhumere, Grazdanov *et al*. reported the different metal sulphide and selenides thin film using electroless deposition method. They studied the optical and electrical properties of Ag_2S thin films[20]. Mo.*et al*. reported Ag_2S with graphene nano composites for supercapacitor applications using hydrothermal synthesis[21].

In this work, we have demonstrated direct growth of Ag_2S on the surface of Nickel (Ni) mesh using CBD technique at a low temperature of 6 °C without addition of any complexing agents like EDTA, TEA or citric acid and binders. Then the prepared Ag_2S materials on Ni mesh were employed directly without any further process for electrochemical characterization. From the electrochemical studies, it observed that the Ag_2S materials showed better performance for energy storage applications.

Results and Discussion

Morphological and elemental analysis. Electrochemical performance of the materials are depends on its morphology. Therefore, the morphology of the binder-free Ag_2S on Ni mesh is observed from the FE-SEM analysis and the micrographs with different magnifications are presented in Fig. 1. The deposition of Ag_2S over the surface of Ni mesh is shown in Fig. 1a and the individual particles attached on the Ni mesh are clearly observed in Fig. 1b. The particles are truncated cubic in structure which agglomerated to form ball like structures and Fig. 1c shows the elemental composition present in the sample using EDAX analysis, it shows the atomic weight percentage of Ag and S was found to be 67.50 and 32.50% which reveals the Ag_2S formation.

Phase structure and functional analysis. To identify the crystalline behaviour as well as phase structure of the synthesized Ag_2S, X-Ray diffraction analysis has been carried out and the obtained diffraction patterns are presented in Fig. 2a. The XRD pattern of the prepared sample shows sharp diffraction pattern indicating that Ag_2S is well crystalline in nature. The observed 2θ values of intense diffraction are 22.38, 25.98, 28.92, 31.55, 34.49, 36.79, 37.71, 40.7, 43.45, 46.28, 53.27° corresponds to lattice planes (−1 0 1), (−1 1 1), (1 1 1), (−1 1 2, (−1 2 1), (1 2 1), (−1 0 3), (0 3 1), (2 0 0), (−1 2 3) and (−2 1 3) of Ag_2S respectively. The measured diffraction angles and interplanar spacing are in close agreement with the standard diffraction pattern of acanthite phase of Ag_2S (JCPDS No.: 01-014-0072). The average crystallite size of the as-synthesized Ag_2S is calculated using

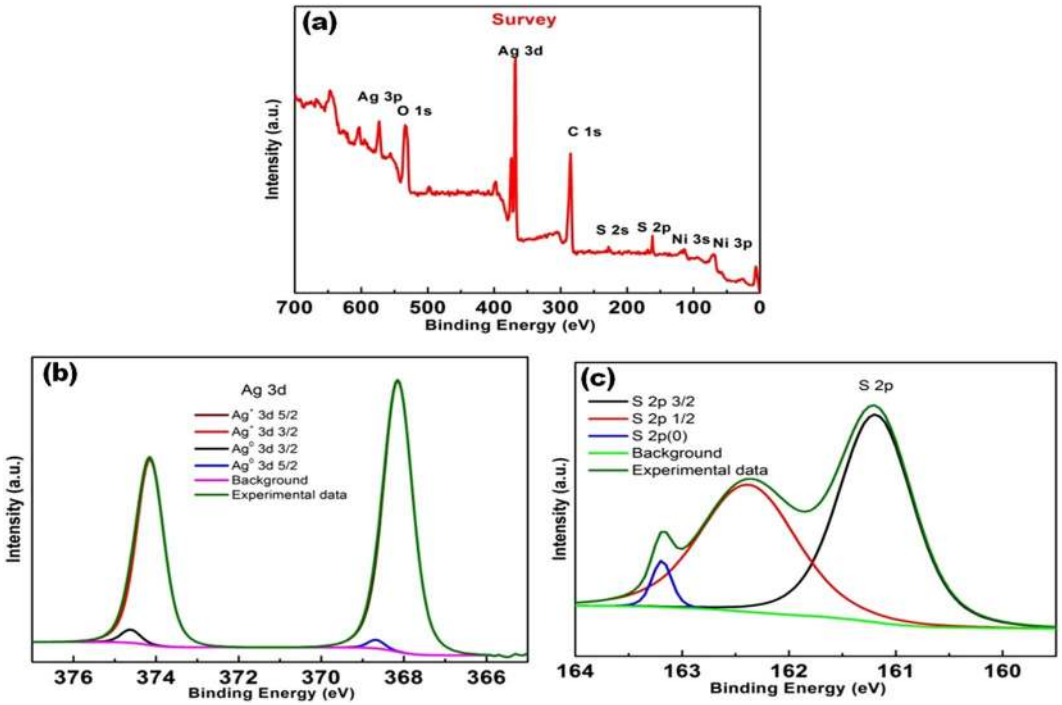

Figure 3. XPS spectrum of Ag_2S nanoparticles (**a**) survey spectrum (**b**,**c**) High resolutionspectra of Ag and S.

Debye Scherer relation and is found to be around 48–86 nm[22]. Mostly, the synthesis of sulphides based materials by chemical approaches results in formation of mixed phase structure because of its complex stoichiometric nature[23]. But in this present case, there is no formation of additional peaks confirming the phase of the synthesized materials.

In order to understand the nature of functional groups present in the synthesized Ag_2S, FT-IR analysis is carried out and the spectra is given in Fig. 2b. The sharp band appears in the region of 1596 cm^{-1}, 1389 cm^{-1} and broad band around 3400 cm^{-1}. The broad band at the region of 3400 cm^{-1} is due to the presence of adsorbed water molecules[24], and the other bands observed at 1596, 1389, and 532 cm^{-1} corresponds to C = S stretching, N-C-N symmetric stretching and N-C-S bending vibrations respectively[25,26]. A peak with relatively weak intensity observed at 665 cm^{-1} corresponds to the sulphur-sulphur bond in metal sulphides[27].

Chemical composition analysis. XPS analysis reveals the information about the chemical state and the elemental composition of the synthesized Ag_2S materials. An extensive scan of survey spectrum of Ag_2S (Fig. 3a) with the physically powerful existence of Ag 3d (365.6 eV, 372.7 eV) and S 2p (16.21 eV, 163.6 eV) doublets along with C 1 s (284.3 eV), O 1 s (534.3 eV) and other Ag- and S- related core-level binding energy and auger peaks. The apparent existence of Ag 3d and S 2p doublets indicates the formation of Ag_2S nanoparticles. High resolution scan of Ag 3d and S 2p core-level spectra are shown in Fig. 3b,c respectively. Ag 3d binding energy spectrum is deconvoluted and fitted with two silver doublets. Binding energy centred at 374.1 eV ($3d_{3/2}$) and 368.1 eV ($3d_{5/2}$) contribute to Ag^+ silver sulphide formation, whereas peaks at 374.6 eV ($3d_{3/2}$) and 368.6 eV ($3d_{5/2}$) are endorsed to Ag°, metallic state of silver in the metal sulphide nanoparticles. A relative shift of about 0.5 eV is observed for the Ag° oxidation state towards high energy as compared to Ag^+ state. All these experimental findings are much in streak with existing values of Ag_2S[28–30].

Related to the Ag 3d, a high-resolution binding energy spectrum of S 2p has been observed (Fig. 3c). The recorded S 2p binding energy spectrum is deconvoluted for spin orbit splitting of metal sulphide S^{2+}, centred on 161.2 eV ($2p_{3/2}$) and 162.3 eV ($2p_{1/2}$). A spin orbit splitting with an intensity ratio of 0.52 (expected theoretical value is 0.5) for S 2p matches with an earlier reported values and suggest the formation of Ag_2S[28,30,31].

Electrochemical measurements. Electrochemical characteristics of fabricated binder-free Ag_2S working electrode are evaluated using cyclic voltammetry (CV), galvanostatic charge/discharge (GCD) and electrochemical impedance spectroscopy (EIS) with a conventional three electrode system. Initially, the CV profile of Ag_2S electrodes is recorded in 20% KOH electrolyte solution with different scan rates of 5–50 mV s^{-1} and the potential window of 0–0.6 V respectively. Before evaluating the electrochemical performance of the Ag_2S deposited over the Ni mesh, the performance of bare Ni mesh has been done for comparative purposes and it is represented as Fig. 4a,b.

The recorded CV curve shapes discernible from the rectangular shape pointing out that the energy storage of Ag_2S electrode impute to the faradaic capacity behaviour with two redox peaks[32,33]. The anodic and cathodic oxidation sweep lies at the range of 0.25–0.45 V and 0–0.2 V respectively (Fig. 5a). As the value of scan rate increases, there exists distortion in the symmetry of the CV curves and at the high scan rate an asymmetrical nature of the

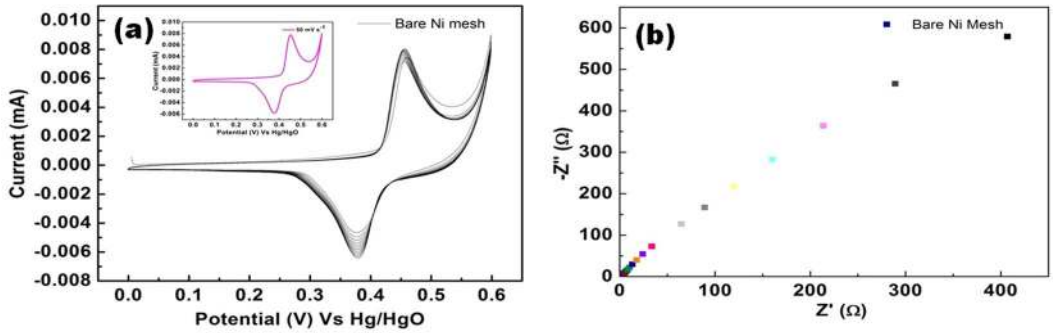

Figure 4. Electrochemical analysis of bare Ni mesh.

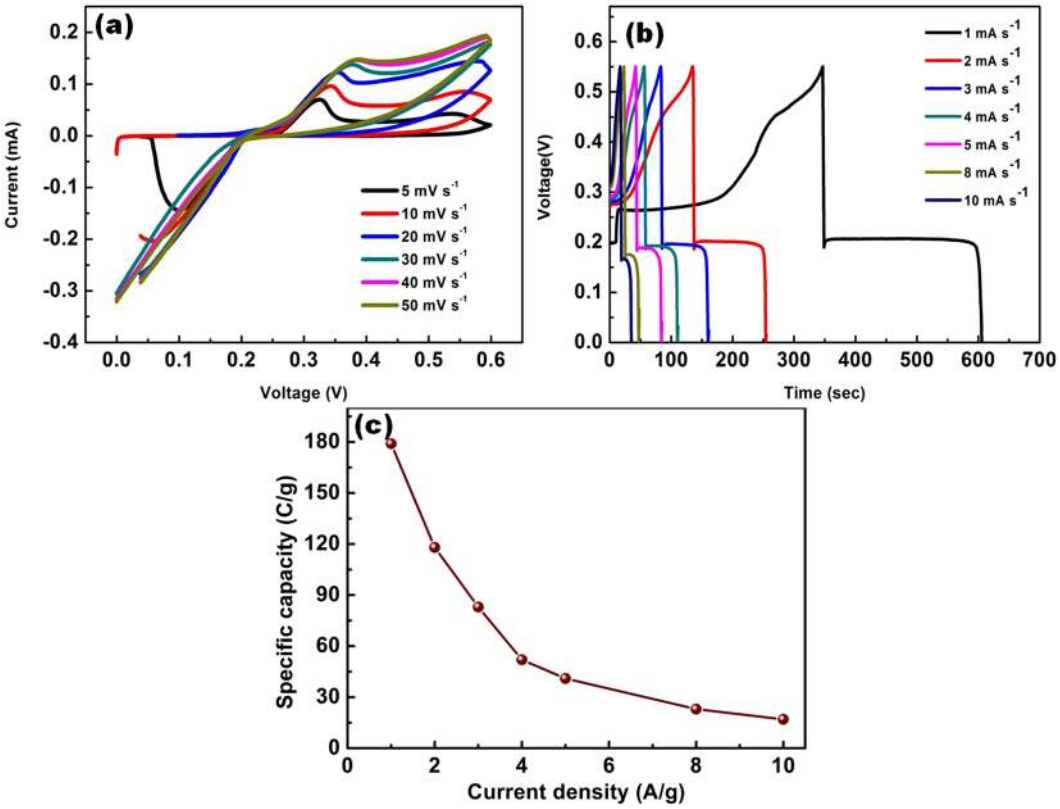

Figure 5. Electrochemical studies of Ag_2S deposited on Ni mesh (**a**) CV profile, (**b**,**c**) CD and Specific capacity profile.

anodic and cathodic peak has been exists which may due to the kinetic irreversibility of the redox process[27]. The electrochemical behavior of Ag_2S electrode in KOH electrolyte solution can be elucidated by following electrochemical reactions:

$$Ag_n^0 \Leftrightarrow Ag_n^+ + e^- \quad (1)$$

$$Ag_2S + OH^- \Leftrightarrow Ag_2S(OH) + e^- \quad (2)$$

Figure 5b shows the GCD profile of the Ag_2S electrode measured at different current densities of 1–10 A/g with the potential window of 0–0.55 V. It clearly shows that there is voltage levelling-off period near 0.2 V in each discharge curve. Non-linear variation of Voltage Vs Time (charge/discharge), further entail a classic faradaic capacity behaviour resultant of occurrence of redox from the redox occurring at the electrode/electrolyte interfaces. The potential window between 0.2–0.5 V appeared to be non-symmetric, insulating battery behaviour showing IR drop. Despite the steep potential drops, prolonged plateau of output voltage is observed in the range

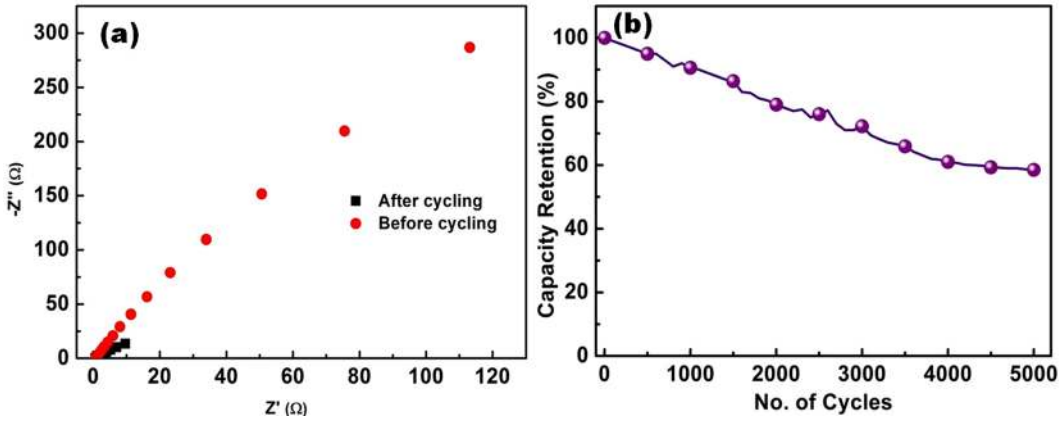

Figure 6. (**a**) EIS spectra and (**b**) Specific capacity retention.

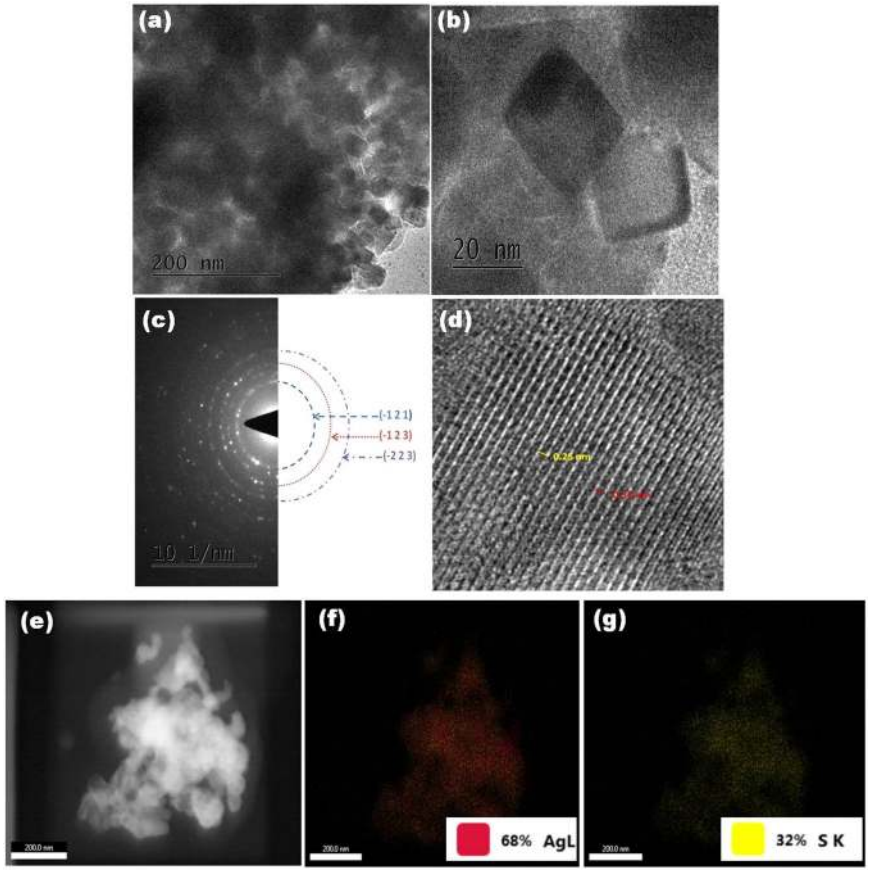

Figure 7. (**a**) HRTEM image, (**b**) higher magnification, (**c**) SAED pattern, (**d**) lattice fringes. (**e**) Elemental mapping of Ag_2S, (**f**) Ag and (**g**) S.

of 0.2 V, which is due to the faradaic process that takes place in Ag_2S electrode[34]. From the obtained GCD profile the specific capacitance can be calculated using the following equation[35]:

$$C_s = \frac{I * \Delta t}{m}$$

Where, C_s is the specific capacitance (F/g), I was the discharge current (A), m is the active mass of the material, Δt is the discharge time (sec). C_s values are calculated from the GCD profile and the results were plotted in Fig. 5c. From Fig. 5c it is evident that the specific capacity drops with increasing current densities. C_s at different current densities of 1, 2, 3, 4, 5, 8 and 10 A/g are calculated and found to be 179, 118, 83, 52, 41, 23 and 17 C/g respectively.

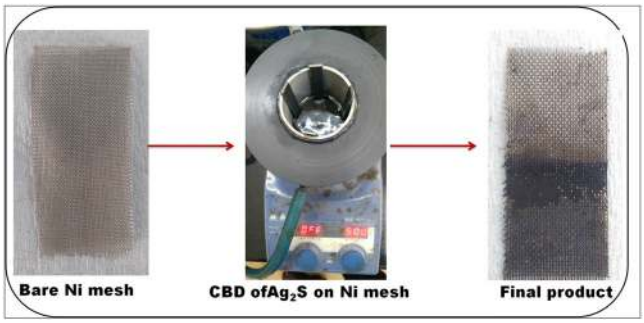

Figure 8. Pictorial representation of Ag_2S deposition on Ni mesh via CBD.

Ag_2S electrode shows a maximum specific capacity of 179 C/g for 1 A/g current density, which seems to be higher compared to other reported sulphur based materials such as CuS (62 F/g), ZnS (32 F/g), WS_2 (40 F/g), RuS_2 (85 F/g)[36–39]. This sort of high specific capacitance can be allocated to its architecture providing rapid electron and ion transfer and easy access to electrolyte ions. The CV and GCD result confirms that the active material Ag_2S are battery type electrode materials. The IR drop in GCD profile features the charge conduction and ion diffusion process. Even operating at higher current rate the charge curve and the discharge counterpart exist to symmetry indicating the good coulombic performance of the device[40].

The rate capability is a prime aspect of consideration in designing high power supercapacitors, which is evaluated from electrochemical impedance spectroscopy (EIS) studies[41,42]. Nyquist plot of Ag_2S electrode, after and before cycling was carried out with frequency ranging from 100 kHz to 100 mHz as shown in Fig. 6a. An intercept with real axis at high frequency represents the series resistance, which is combination of ionic resistance of the electrolyte, electronic resistance of the electrode materials and interface resistance[43]. It is evident that there is no remarkable change in the external sheet resistance (ESR) after the cycling test, which indicates high ionic conductivity of the supercapacitors. A sharp increase of impedance towards lower frequency indicates the pure capacitive behaviour which arises from diffusion of redox species. The stability of the electrode materials plays a vital role for the practical applications of supercapacitors. Therefore, the cycling stability of the electrode was evaluated at 10 A/g for 5000 cycles as shown in Fig. 6b. The capacity retention of the active materials (Ag_2S) maintains reasonable stability over the prolong period of 5000 cycles. It is evident from the data that Ag_2S can serves as a remarkable electrode material in the development of high performance electrochemical behaviour owing to its excellent behaviour with good cyclability and high retention capacity.

Microstructure analysis. The microstructure analysis of Ag_2S material was carried out using HR-TEM analysis. The micrograph shown in Fig. 7a,b confirmed that as-synthesized Ag_2S are smaller particles in the order of nanometer (nm) in range with the size of 20–25 nm. Figure 7c represents the SAED pattern of Ag_2S nanoparticles, the observed ring profile was indexed and it corresponds to the plane of (−1 2 1), (−1 2 3), (−2 2 3). The high intensity spots observed in the inner ring matches 100% with the plane of (−1 2 1) confirming Ag_2S nanoparticles are polycrystalline in nature. The lattice fringes of the Ag_2S nanoparticles is clearly seen in Fig. 7d with the d-spacing of about 0.25 nm which closely matched to the standard value (0.260 nm) and indexed to the (−1 2 1) lattice plane. Figure 7e–g shows elemental mapping profile of Ag and S present in the sample. The mapping results show that Ag and S are uniformly distributed in the entire sample.

Conclusion

In conclusion, we have reported the deposition of nanocubic Ag_2S on the surface of Ni mesh by a simple and cost effective chemical bath deposition for the supercapacitor applications. The acanthite phase of Ag_2S with good crystalline is confirmed from the XRD studies. The XPS studies emphasize the formation of Ag_2S is in nearly stochiometric form. The electrochemical studies of Ag_2S electrode show a considerable supercapacitance performance value of 179 C/g at 1 A/g. In addition, the Ag_2S prepared by this method serves as an additive free electrode and exhibits its better performances in electrochemical studies. Thus, these results imply promising electrochemical behaviour of Ag_2S electrode towards cutting edge applications in energy storage sectors.

Methods

Materials and characterization. Silver Nitrate ($AgNO_3$, 98%, SRL, INDIA); Thiourea (CH_4N_2S, 98%, Merck KGaA, Germany); Ammonia Solution (NH_3, 25% GR, Merck, INDIA); Nickel Mesh (Ni) and Deionised water. All the chemicals and reagents used in this experiment are procured commercially with analytical grade and are used as such.

The phase structure and the crystalline behaviour of the fabricated Ag_2S thin film was deliberated using X-Ray diffraction (XRD, Bruker, D8 Advance) with Cu K_α radiation ($\lambda = 0.15406$ nm) at a scanning rate of 0.05 s^{-1}. Particle size of the sample was analyzed using High Resolution Transmission Electron Microscopy (HRTEM, Tecnai 20, G2, FEI) operating at 200 kV with capable of an information limit of 0.14 Å. The oxidation states of Ag and S in the Ag_2S films were examined using X-ray Photoelectron Spectrometer (XPS, Thermo scientific model: MATLAB 2000), operating with an Mg source with $h\upsilon = 1253.6$ eV. Morphology of Ag_2S deposited on Ni mesh

was observed using Field Emission Scanning Electron Microscopy (FESEM, Carl Zeiss microscope, surpa-55VP). Prior to the analysis, surface of the samples were sputtered using gold (Au) for better electrical conductivity. The functional group present in the Ag_2S sample was analysed using Fourier-transform Infrared Spectroscopy (FTIR, FTIR-6300 Japan, Model-Tensor 27).

Electrochemical characteristics of the binder-free Ag_2S were evaluated using three electrodes configurations with 3.6 M KOH aqueous electrolyte. Ni mesh coated with Ag_2S served as a working electrode, Platinum wire as counter electrode and Hg/HgO as reference electrode.

Fabrication of binder-Free Ag_2S electrodes. In a typical fabrication of Ag_2S on Ni mesh, an equimolar (0.1 M) ratio of silver nitrate and thiourea has been taken as source for silver and sulphur. Initially, the Ni mesh was placed on the bath which is maintaining at 6 °C temperature. Prior to addition of precursors Ni mesh undergoes treatment to remove native oxides as per earlier report[44]. Then the prepared silver nitrate solution was added on to the bath followed by addition of sulphur source (thiourea). To maintain the solution in basic nature (pH~9), few drops of ammonia solution was added to the homogeneous solution. An additional feature of this synthesis methodology was that it does not require any binders such as nafion or triton-X 100 for deposition of materials on the surface of Ni mesh electrode. After the experiment the loading of active materials on the Ni mesh was calculated by weighing the weight difference between before and after loading. The loading of active materials was found to be 0.6 mg. The schematic pictorial representation for CBD of Ag_2S on Ni mesh is shown in Fig. 8.

Data Availability

Readers can access the data via contact to the authors.

References

1. Lee, S. W. *et al*. High-power lithium batteries from functionalized carbon-nanotube electrodes. *Nature Nanotechnology* **5**, 531–537 (2010).
2. Guo, S. & Dong, S. Graphene nanosheet: synthesis, molecular engineering, thin films, hybrids, and energy and analytical applications. *Chemical Society Reviews* **40**, 2644–2672 (2011).
3. Arulraj, A., Ramesh, M., Subramanian, B. & Senguttuvan, G. *In-situ* temperature and thickness control grown 2D-MoS_2 via pulsed laser ablation for photovoltaic devices. *Solar Energy* **174**, 286–295 (2018).
4. Conway, B. E. Transition from "Supercapacitor" to "Battery" behavior in electrochemical energy storage. *Journal of the Electrochemical Society* **138**, 1539–1548 (1991).
5. Conway, B. Electrochemical Supercapacitors: Scientific Fundamentals and Technological Applications, Springer, https://doi.org/10.1007/978-1-4757-3058-6 (1999).
6. Simon, P. & Gogotsi, Y. Materials for electrochemical capacitors. *Nature materials* **7**, 845–854 (2008).
7. Shuijing, S., Liao, C., Hafez, A. M., Zhu, H. & Wu, S. Two-dimensional MXenes for energy storage. *Chemical Engineering Journal* **338**, 27–45 (2018).
8. Miller, J. R. & Simon, P. Electrochemical capacitors for energy management. *Science* **321**, 651–652 (2008).
9. Wang, G., Zhang, L. & Zhang, J. A review of electrode materials for electrochemical supercapacitors. *Chemical Society Reviews* **41**, 797–828 (2012).
10. Huang, K.-J., Wang, L., Zhang, J.-Z., Wang, L.-L. & Mo, Y.-P. One-step preparation o layered molybdenum disulfide/multi-walled carbon nanotube composites for enhanced performance supercapacitor. *Energy* **67**, 234–240 (2014).
11. Feng, J. *et al*. Metallic Few Layered VS_2 ultrathin nanosheets: high two-dimensional conductivity for in-plane supercapacitors. *Journal of the American Chemical Society* **133**, 17832–17838 (2011).
12. Huang, K.-J., Zhang, J.-Z. & Fan, Y. Preparation of layered $MoSe_2$ nanosheets on Nifoam substrate with enhanecd supercapacitor performance. *Materials Letters* **152**, 244–247 (2015).
13. Zhang, Y. *et al*. Facile fabrication of flower like $CuCo_2S_4$ on Ni foam for supercapacitor applications. *Journal of Materials Science* **52**, 9531–9538 (2017).
14. Rui, X., Tan, H. & Yan, Q. Nanostructured metal sulfides for energy stotage. *Nanoscale* **6**, 9889–9924 (2014).
15. Chen, S. *et al*. Tuning the electrochemical behaviour of Co_xMn_{3-x} sulphides by varying different Co/Mn ratios in supercapacitors. *Journal of Materials Science* **52**, 6687–6696 (2017).
16. Munoz, J. *et al*. Electrochemical behaviour of chalcopyrite in the presence of silver and sulfolobus bacteria. *Journal of applied electrochemistry* **28**, 49–56 (1998).
17. Brelle, M. C. & Zhang, J. Z. Femtosecond study of photo-induced electron dynamic in AgI and core/shell structured AgI/Ag_2S and AgBr/Ag_2S colloidal nanopartciles. *The Journal of chemical physics* **108**, 3119–3126 (1998).
18. Hsu, T.-Y., Buhay, H. & Murarka, N. P. Characteristics and Application of Ag_2S Films The Millimeter Wavelength region, *Millimeter Optics*, **259**, https://doi.org/10.1117/12.959640 (1981).
19. Dhumure, S. & Lokhande, C. Solution growth of silver sulphide thin films. *Materials chemistry and physics* **27**, 321–324 (1991).
20. Grozdanov, I. A simplest and low-cost technique for electroless deposition of chalcogenide thin films. *Semiconductor science and technology* **9**, 1234 (1994).
21. Mo, Z. *et al*. Graphene sheets/Ag_2S nanocomposites: Synthesis and their application in supercapacitor materials. *Materials Letters* **68**, 416–418 (2012).
22. Klug, H. P. & Alexander, L. E. X-ray diffraction procedures, Wiley New York (1954).
23. Huang, G., Chen, T., Wang, Z., Chang, K. & Chen, W. Synthesis and electrochemical performances of cobalt sulphides/graphene nanocomposites as anode material of Li-ion battery. *Journal of Power Sources* **235**, 122–128 (2013).
24. Arulraj, A., Bhuvaneswari, S., Senguttuvan, G. & Ramesh, M. Solution processed inverted organic bulk heterojunction solar cells under ambient air atmosphere. *Journal of Inorganic and Organomettalic Polymers and Materials* **28**, 1029–1036 (2018).
25. Jeevanandam, P., Koltypin, Y., Gofer, Y., Diamant, Y. & Gedanken, A. Sonochemical synthesis of nanocrystallites of ruthenium sulphide, RuS1.7. *Journal of Materials Chemistry* **10**, 2769–2773 (2000).
26. Li, Y., Li, N., Yanagisawa, K., Li, X. & Yan, X. Hydrothermal synthesis of highly crystalline RuS_2 nanoparticles as cathodic catalysts in the methanol fuel cell and hydrochloric acid electrolysis. *Materials Research Bulletin* **65**, 110–115 (2015).
27. Lee, J. W., Ahn, T., Soundararajan, D., Ko, J. M. & Kim, J.-D. Non-aqueous approach to the preparation of reduced graphene oxide/α-$Ni(OH)_2$ hybrid composites and their high capacitance behaviour. *Chemical Communications* **47**, 6305–6307 (2011).
28. Saber, T. M. H. & El Warraky, A. A. AES and XPS study on the tarnishing of silver in alkaline sulphide solutions. *Journal of Materials Science* **23**, 1496–1501 (1988).
29. Jiang, D., Chen, L., Xie, J. & Chen, M. Ag_2S/g-C_3N_4 composite photocatalysts for efficient Pt-free hydrogen production. The co-catalyst function of Ag/Ag_2S formed by simultaneous photodeposition. *Dalton Transactions* **43**, 4878–4885 (2014).

30. Karthick, R., Arulraj, A., Selvaraj, M. & Ramesh, M. Free-standing graphene/NiMoS paper as cathode for solid-state dye sensitized solar cells. *Journal of Colloid and Interface Science* **530**, 179–188 (2018).
31. Fan, W., Jewell, S., She, Y. & Leung, M. K. *In situ* deposition of Ag-Ag_2S hybrid nanoparticles onto TiO_2 nanotube arrays towards fabrication of photoelectrodes with high visible light photoelectrochemical properties. *Physical Chemistry Chemical Physics* **16**, 676–680 (2014).
32. Dong, C. *et al*. 3D binder-free Cu_2O@Cu nanoneedle arrays for high-performance asymmetric supercapacitors. *Journal of Materials Chemistry A* **2**, 18229–18235 (2014).
33. Zhang, J. T., Liu, S., Pan, G. L., Li, G. R. & Gao, X. P. A 3D hierarchical porous $Ni(OH)_2$/graphite nanosheet composite as an electrode material for supercapacitors. *Journal of Materials Chemistry A* **2**, 1524–1529 (2014).
34. Arora, Y. *et al*. Nanostructured MoS_2/$BiVO_4$ composites for energy storage applications. *Scientific reports* **6**, 36294 (2016).
35. Yang, Z. *et al*. Controllable preparation of multi-shelled NiO hollow nanospheres via layer-by-layer self-assembly for supercapacitor application. *Journal of Power Sources* **246**, 24–31 (2014).
36. Krishnamoorthy, K., Veerasubramani, G. K., Radhakrishnan, S. & Kim, S. J. Preparation of copper sulfide nanoparticles by sonochemical method and study on their electrochemical properties. *Journal of nanoscience and nanotechnology* **15**, 4409–4413 (2015).
37. Ramachandran, R. *et al*. Solvothermal synthesis of zinc sulfide decorated graphene (ZnS/G) nanocomposites for novel supercapacitor electrodes. *Electrochimica Acta* **178**, 647–657 (2015).
38. Mayorga-Martinez, C. C., Ambrosi, A., Eng, A. Y. S., Sofer, Z. & Pumera, M. Transition metal dichalcogenides (MoS_2, $MoSe_2$, WS_2 and WSe_2) exfoliation technique has strong influence upon their capacitance. *Electrochemistry Communications* **56**, 24–28 (2015).
39. Krishnamoorthy, K., Pazhamalai, P. & Kim, S. J. Ruthenium sulfide nanoparticles as a new pesudocapacitive material for supercapacitor. *Electrochimica Acta* **227**, 85–94 (2017).
40. Xie, J. *et al*. Puzzles and confusions in supercapacitor and battery: Theory and solutions. *Journal of Power Sources* **401**, 213–223 (2018).
41. Singh, M. K., Suleman, M., Kumar, Y. & Hashmi, S. An novel configuration of electrical double layer capacitor with plastic crystal based gel polymer electrolyte and graphene nano-platelets as electrodes: a high rate performance. *Energy* **80**, 465–473 (2015).
42. Tamilarasan, P. & Ramaprabhu, S. Graphene based all-solid-state supercapacitors with ionic liquid incorporated polyacrylonitrile electrolyte. *Energy* **51**, 374–381 (2013).
43. Shi, J., Li, X., He, G., Zhang, L. & Li, M. Electrodeposition of high-capacitance 3D CoS/graphene nanosheets on nickel foam for high-performance aqueous asymmetric supercapacitors. *Journal of Materials Chemistry A* **3**, 20619–20626 (2015).
44. Wang, B. *et al*. Integration of network-like porous $NiMoO_4$ nanoarchitectures assembled with ultrathin mesoporous nanosheets on three dimensional graphene foam for highly reversible lithium storage. *Journal of Materials Chemistry A* **3**, 13691–13698 (2015).

Acknowledgements

Author Dr. M. Ramesh gratefully acknowledges Department of Science and Technology (DST) for awarding INSPIRE Faculty award (DST/INSPIRE/04/2015/002860) and Director, CSIR-CECRI for implementation of award. Author Mr. A. Arulraj extends his sincere thanks to the Director, CSIR- CECRI, Karaikudi for providing facilities to carry out the research work. Mr. A. Arulraj express gratitude for his supervisor Prof. G. Senguttuvan, UCE-BIT Campus, Tiruchirappalli for his constant support in this mansucript.

Author Contributions

A.A. and M.R. conceived the idea of the work. A.A. have done all the synthesis and characterization work. N.I. assists in performing and analysing the supercapacitor cells. V.R. helped in preparing the manuscript. M.R. supervised the overall work.

Additional Information

Competing Interests: The authors declare no competing interests.

Publisher's note: Springer Nature remains neutral with regard to jurisdictional claims in published maps and institutional affiliations.